Atlas Journal of Materials Science 2020, pp. 90–98
doi: 10.5147/ajms.v0i0.217

Performance of Hybrid $SnO_2/Li_2FeMn_3O_8$ Nanostructured Electrode for Efficient Li-ion Storage Application

Samuel A. Danquah[1*], Sangram K. Pradhan[1], Wondwossen D. Arasho[2], and Messaoud Bahoura[1,3]

[1] Center for Materials Research, Norfolk State University, Norfolk, VA 23504, USA; [2] Chemistry Department, Norfolk State University, Norfolk, VA 23504, USA; [3] Engineering Department, Norfolk State University, Norfolk, VA 23504, USA

Received: May 5, 2020 / Accepted: June 14, 2020

Abstract

$Li_2FeMn_3O_8$ (LFMO) nanocomposite material for Li-ion battery is synthesized using the chemical combustion method. To fabricate a hybrid nanostructure electrode, LFMO is coated on tin oxide (SnO_2) nanorods (NR), which is grown using a vapor-liquid-solid (VLS) technique on a steel substrate. The surface morphology of the hybrid nanostructure electrode confirms that single-crystalline SnO_2 nanorods are grown vertically with spine-like structures, a few microns in length, as evident from field emission scanning electron microscope image. The electrochemical performance of SnO_2/LFMO shows very interesting characteristic with enormous charge storage capability. The coin cell shows improved capacity with a higher number of charging and discharging cycles. This SnO_2/LFMO hybrid composite electrode shows better specific capacitance value as compared to the pristine SnO_2 electrode.

Introduction

Compared to the various types of batteries, lithium-ion batteries (LIBs) are one of the most currently used energy storage devices. Due to their high energy density and long cycle stability, they are used in numerous applications such as consumer electronics, electric vehicles, and power grids to name a few. The quest to improve the performance of LIBs has sparked a lot of research interest in the field of energy storage, especially the search for new electrode materials and optimization of already existing electrodes materials.

The performance of LIBs relies greatly on the properties and structure of the electrode material for lithium storage (Wang et al., 2013; Wang et al., 2012; Wang et al., 2013). Nanostructured electrodes are of great importance in lithium-ion storage because of their large surface area for lithium insertion channels as well as quick lithium-ion diffusion (Wang et al., 2013; Liu et al., 2012; Xu et al., 2012). Also, carbonaceous materials have been used to serve as a volume change buffers and good electron conductors to enhance the electrochemical performance of SnO_2 nanocomposites (Wang et al., 2015). One such electrode material is tin dioxide (SnO_2) nano-

* Corresponding author: s.a.danquah@spartans.nsu.edu

rods because of its high theoretical capacity of (~782 mAhg-1), low cost, abundance and relatively low charge-discharge plateau compared to other metal oxides (Wang et al., 2015; Poizot et al., 2000; Tarascon et al., 2001; Arico et al., 2005). Besides, SnO_2 is a semiconductor with good lithium storage properties, exhibits nontoxic and nonreactive behaviors owing to its excellent electrical conductivity. Desirable properties of SnO_2 are believed to improve the electrochemical performance of cathode materials when applied as a coating (Carvajal et al., 2017; Guan et al., 2014; Hudaya et al., 2014). Besides these advantages, SnO_2 electrodes also encounter a few issues such as (i) severe electrode pulverization and capacity fading during the cycling process as a result of 200% volume expansion, which occurs during lithiation and de-lithiation process; (ii) relatively low discharging capability due to low electrical conductivity, which reduces the electron transport; and (iii) poor Coulombic efficiency due to irreversible conversion reaction during initial lithiation process resulting in additional cathode material consumptions. There is a myriad of research efforts to provide solutions to problems that affect the surface area and the lithium-ion kinetics in a positive direction. This is achieved via the use of surface modification such as nanorods, nanowires, and nanotubes (Wang et al., 2015).

LFMO is a lithium-rich cathode material with a high atomic ratio of extractable lithium to the transition metal, which is noted to provide a high discharge capacity (Penki et al., 2016). The LFMO is one of the efficient cathode materials that deliver a specific capacity of 103 mAhg-1, which is 70 % of its theoretical capacity value with 83 % of Coulombic efficiency during the first cycle. Also, the LFMO exhibits two groups of distinct plateaus at 4.0 V and 4.9 V for discharge and 4.1 V and 5.0 V for charge (Penki et al., 2016). Furthermore, the LFMO contains the majority of iron and manganese without cobalt, which makes it environmentally friendly, and less expensive than Co and Ni-based cathodes (Zhao et al., 2016; Tabuchi et al., 2005). Nevertheless, LFMO cathode materials, reported in the literature, exhibit low rate capabilities due to their low electronic and ionic conductivities, which limit their practical application (Zhao et al., 2016; Pan et al., 2018; Si et al., 2015). Cation-doping and surface modifications, by coating with carbon, have been modified to improve the electrochemical performances of LFMO (Yuge et al., 2016; Wu et al., 2015; Wang et al., 2016). Considering the properties of the SnO_2 nanorods and the LFMO stated above, there would be a trade-off, if the composite material can be prepared out of these two materials. Therefore, the incorporation of LFMO into the SnO_2 nanorods forming a composite electrode, could potentially enhance the electrochemical performance of the battery for better energy storage application. Hudaya et al. reported on SnO_2 thin film coating on $LiCoO_2$ cathode material. The SnO_2 coating increases the initial discharge capacity of pristine $LiCoO_2$ from 172 to 183 mAhg-1 at 1C (Hudaya et al., 2014). Furthermore, other researchers used insulating materials or semiconductive materials such as ALF_3, Al_2O_3, TiO_2, ZnO, Li_4SiO_4, $LiAlO_2$, and SnO_2 as effective coating materials for cathode electrode in the lithium-ion battery. These coatings do not only prevent the active substances from diffusion and dissolution in electrolyte but also improve the electronic conductivity as well as structural stability (Wang et al., 2019; Yang et al., 2012; Lee et al., 2013; Wang et al., 2015; Dai et al., 2016; Lai et al., 2016; He et al., 2017; Srur-Lavi et al., 2017; Liua et al., 2018; Zheng et al., 2018; Xie et al., 2019). The advantage of the vapor-liquid-solid (VLS) technique, used in growing the SnO_2, compared to the other SnO_2 coating is that you can grow highly oriented vertically dense nanorods with easy size tunability and no sophisticated or expensive equipment, such as chemical vapor deposition (CVD).

Materials and Methods

The synthesis procedure and the chemicals used to fabricate the SnO_2 nanorods as well as the LFMO composite is shown in Figure 1. SnO_2 is synthesized on a cleaned stainless-steel disc substrate using $ZnCl_2$ and $SnCl_2$ powders in a ratio of 4:1 as source materials. The $ZnCl_2$ and $SnCl_2$ were mixed thoroughly in an alumina boat and the cleaned stainless-steel disc substrate is placed on top of a glass slide at approximately 1.6 cm from the bottom of the alumina boat. The alumina boat with the mixture of $ZnCl_2$ and $SnCl_2$ is put inside a furnace in the presence of oxygen under controlled temperature. The furnace is allowed to cool down to room temperature naturally after it stayed constant at 510 ^oC for 10 minutes before the removal of the sample. The ZnO grown dur-

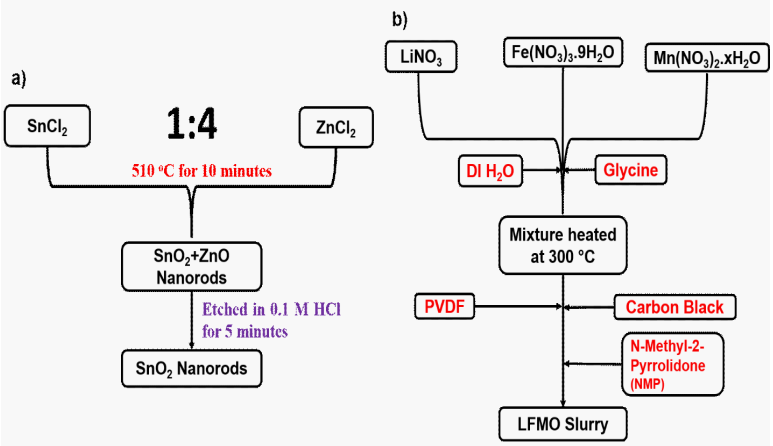

Figure 1. Schematic representation for the synthesis of (a) SnO_2 nanorods using VLS technique and (b) LFMO powder using wet chemical technique.

ing this process is etched out with a 0.1 M HCl for 5 minutes, which allowed only the SnO_2 nanorods to remain on the stainless-steel plate (Carvajal et al., 2017). Field emission scanning electron microscope (FESEM) was used to confirm the growth of the SnO_2 nanorods.

Furthermore, the carbon black and PVDF in a mass ratio of 1:1 is mixed in an NMP to form slurry and coated on the grown SnO_2 nanorods. It is then air-dried and further dried at 80 °C for 10 hours in the vacuum oven to form the electrode.

After the successful growth of the vertical single-crystalline SnO_2 nanorods, the LFMO is subsequently synthesized via a chemical route with modification (Poizot et al., 2000). Lithium nitrate, iron nitrate, and manganese nitrate compounds are used. The mass of the individual compounds is determined by stoichiometric calculations using the molar ratio of 2:1:3. The resulted combination is then mixed with glycine in a molar ratio of 2:1. Thereafter, the whole mixture is dissolved in de-ionized water and heated at a temperature of 300 °C for a combustion reaction (Han et al., 2016). A sudden ignition occurred after the evaporation of the solution leaving the LFMO powder in the beaker. Due to the vigorous nature of the combustion reaction, all the syntheses were done under the fume hood. The LFMO powder is transferred from the beaker into a ceramic container and was further annealed at 700 °C in a furnace for 2 hours to eliminate other volatile content.

The annealed LFMO is mixed with carbon black (good electron conductor), polyvinylidene fluoride (PVDF binder) in a mass ratio percentage of 80:10:10, after which N-methyl-2-pyrrolidone (NMP) is added to obtain slurry in a ratio of 1:2 by weight of solids to liquids. The surface area of the powders greatly affects the viscosity of the slurry. Therefore, the larger the surface area, the thicker the slurry. A slurry is placed on the stirrer overnight for thorough mixing. The resulting slurry is coated on SnO_2 nanorods deposited on the stainless-steel substrate using the doctor blade technique to form the electrode and allowed to dry in air overnight. Furthermore, the electrode on the steel substrate is dried in a vacuum oven at 90 °C for 12 hours. The stainless steel is pre-weighed and post-weighed to determine the active mass of the electrode. The SnO_2 and SnO_2/LFMO composite are used as a cathode electrode to construct an individual coin cell for this work.

The mass ratio of the SnO_2 to $Li_2FeMn_3O_8$ for this study was 1:9 due to the different growth techniques. The SnO_2 is grown in a film, hence, its lightweight whiles LFMO is synthesized in a powder form to prepare the slurry.

Lithium foil is used as an anode electrode and 1 M of lithium hexafluorophosphate ($LiPF_6$) in 1:1 ratio of propylene carbonate (PC) and dimethyl carbonate (DMC) as the electrolyte. The coin cell is left to sit for three days to allow the liquid electrolyte to diffuse via the separator before the electrochemical testing. BST8-WA (MTI corp.) eight-channel battery analyzer is used to analyze the coin cell to determine the cycling performance and its capacity. The channel of the analyzer has independent constant-current and constant-voltage source in a range of 0.005 mA-1.0 mA up to 5 V that is programmed and controlled by computer software.

The discharge specific capacity is calculated by the

battery analyzer system from the discharge curves using the following equation:

Discharge Specific Capacity = [I(mA)×t(h))/(m(g)]

Where I(mA) is the discharge current, t(h) is the discharge time consumed in the voltage range and m(g) is the mass of active materials of the electrode (Jiang et al., 2011). While Coulombic efficiency of any battery is the ratio of charge output to charge input. The calculation of the Columbic efficiency is given by the formula below:

Columbic Efficiency = [Discharge Capacity)/(Charge capacity)×100%]

Thermogravimetric analysis (TGA) is performed to assess the thermal stability of the LFMO raw material since the electrical resistance of conductors could be influenced by temperature (Lacy, 2011). Approximately 5 mg of the sample is placed in a platinum crucible and then placed into a thermogravimetric analyzer. Nitrogen gas of flowrate (30 mL) is allowed into the pyrolyzing unit to ensure an oxygen-free atmosphere. The sample is heated from room temperature to 900 °C at a heating rate of 10 °C/min. It is relevant to know the performance of LFMO as it could be disposed off in the incineration waste plant, which will in turn affect the environment.

The Brunauer-Emmett-Teller (BET) surface area, the pore volume, and the pore size of the new and used catalysts are measured using Quantachrome (NOVA 200e) surface area analyzer having degassed at 300 °C for 3 hours, adsorbed, and desorbed with N_2 at -196 °C. The surface area is evaluated using a multi-point BET model. The pore size distribution is obtained from the desorption isotherm using Barret-Joyner-Halenda (BJH) model (Asiedu et al. 2019; Lowell et al., 2006) while the total pore volume is calculated at a relative pressure (P/P_o) range of 0.0-1.0.

Results and Discussion

FESEM technique is used to verify the morphology of SnO_2 nanorods before the coating of the LFMO onto it. The images, shown in Figure 2(a-b), reveal that SnO_2 is single crystalline in nature and grew vertically with spine-like structures in the range of few microns in length. The FESEM images of the LFMO electrode, Figure 2(c-d), did not exhibit any distinctive shapes or particular arrays, however, it forms an aggregate with particles growing on top of each other. Although LFMO aggregates, when the size is decreased from 5 µm to 2 µm, the pores within the LFMO electrode are still visible. LFMO spread evenly on the SnO_2 nanorods, via doctor blade technique, exhibiting high porosity, as seen in Figure 2(e-f). However, the SnO_2 nanorods are not noticeable in the images. This might be due to the large surface area of LFMO. In addition, the increase in porosity of LFMO/SnO_2 will help to improve the surface area

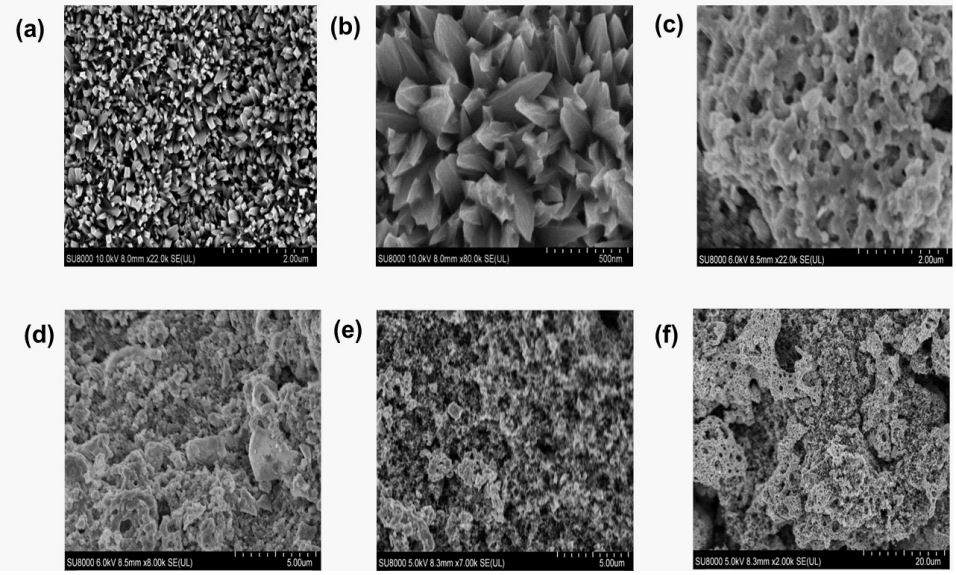

Figure 2. Surface morphology at different magnifications of (a-b) pristine SnO_2, (c-d) pristine LFMO, and (e-f) SnO_2/LFMO composite electrodes.

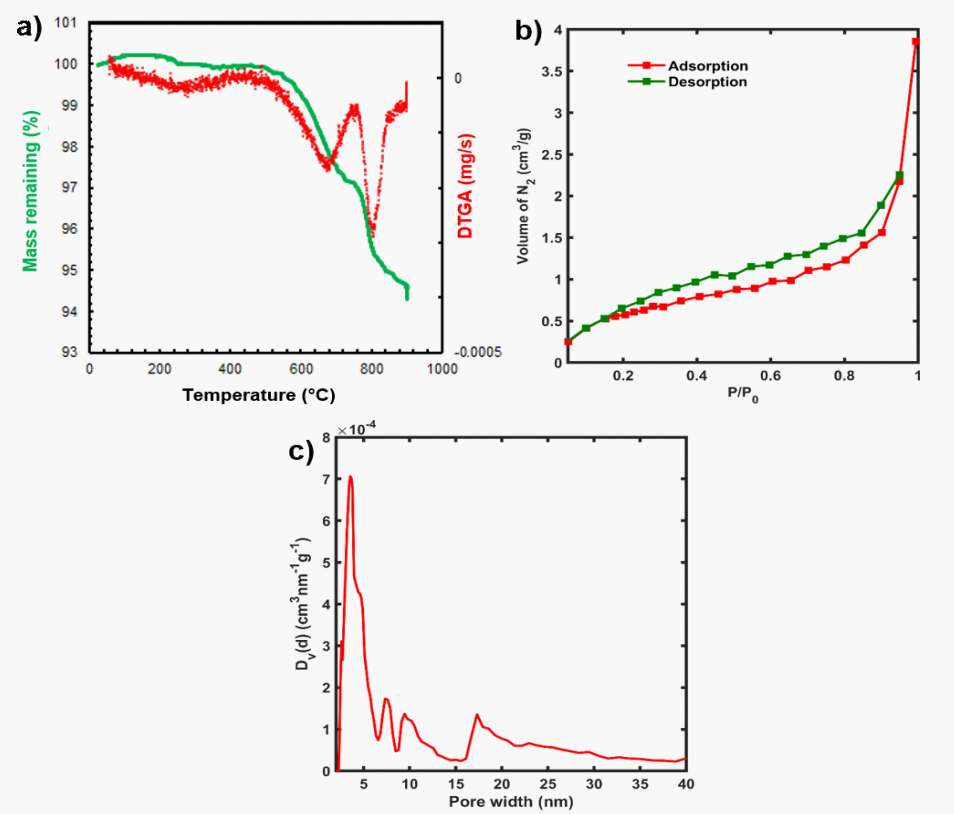

Figure 3. (a) TGA curve for LFMO powder, (b) Adsorption-desorption isotherm curves of LFMO and (c) pore size distribution of LFMO.

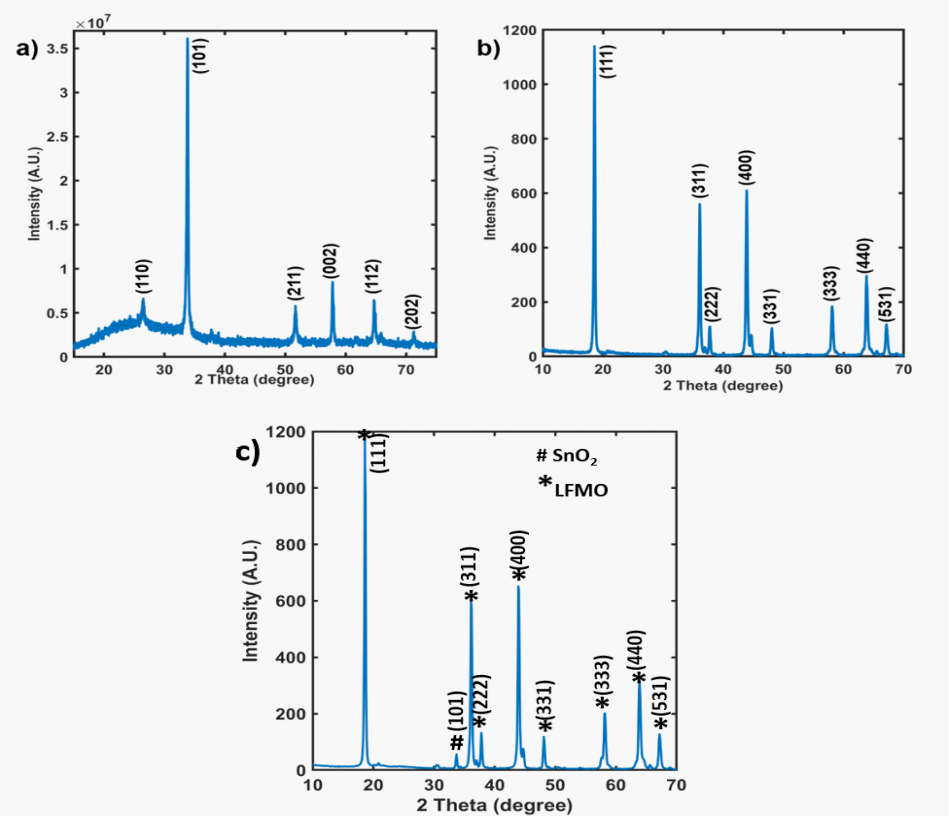

Figure 4. (a) XRD pattern of SnO_2 nanorods and (b) XRD pattern of LFMO powder. (c) XRD pattern of SnO_2/LFMO composite.

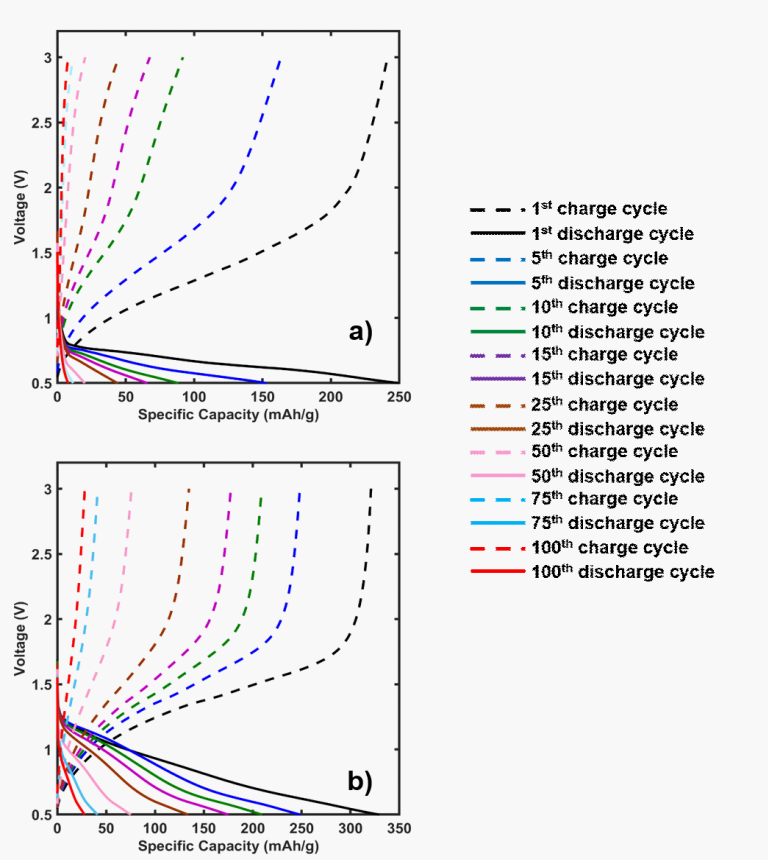

Figure 5. Discharging and charging cycles of Li-ion coin cell battery made up of (a) SnO_2 electrode, and (b) SnO_2/LFMO composite electrode.

for the lithiation and the delithiation process.

Figure 3 (a) highlights the TGA of LFMO as it is heated from room temperature to 900 °C. It is observed that LFMO remained stable between 25-220 °C. It could, therefore, be inferred that the electrical or internal resistance of the material remains unchanged at ambient conditions where the battery is tested. Between 220 °C and 900 oC, LFMO lost nearly 6% of its original mass, which could be traceable to the PVDF binder. The maximum rate of decomposition is experience at 800 °C, which is close to the normal incineration temperature of batteries (D3242-11, 2017; Ebin et al, 2017). This means even if the LFMO ends up at an incineration plant, its environmental emissions would be insignificant compared to the emission of a conventional battery, which loses approximately 80% of its mass into the atmosphere during incineration (Patel et al., 2016).

Figure 3(b) shows the adsorption and desorption of N_2 on the LFMO. It can be observed that as the pressure increased, the volume of N_2 adsorbed increase until the pores in the LFMO became saturated, as indicated by the desorption curve. Decreasing the pressure resulted in the evaporation of the adsorbed N_2 and the decrease in the amount of N_2 in the pores, as shown by the desorption isotherm. This type of hysteresis depicts a type 1 and 4 isotherm, according to the International Union of Pure and Applied Chemistry [19]. It is also observed that the surface area and pore volume for LFMO are 2.018 m^2/g and 4×10^{-3} cm^3/g, respectively. The modal pore width is registered to be 35.5 Å (Figure 3c), which shows that the LFMO is microporous (Asiedu et al., 2019).

To further study the phase composition of the SnO_2 nanorods and the LFMO material, X-ray diffraction is performed with Cu K-alpha radiation at 40 kV and 40 mA. Figure 4 (a) shows XRD patterns of SnO_2 nanorods on a glass substrate. The diffraction peaks reveal that the SnO_2 has a strong peak on the (101) plane. In addition, the nanorods are well crystalized as results of the enhanced (002) peaks, which grows the crystals on the (001) direction. The XRD pattern also matched with the JCPDS Card #41-1445, which is in an agreement with the results of Sharma et al. (Sharma et al., 2018). In addition, the SnO_2 exhibited a rutile structure, which is associated with tetragonal

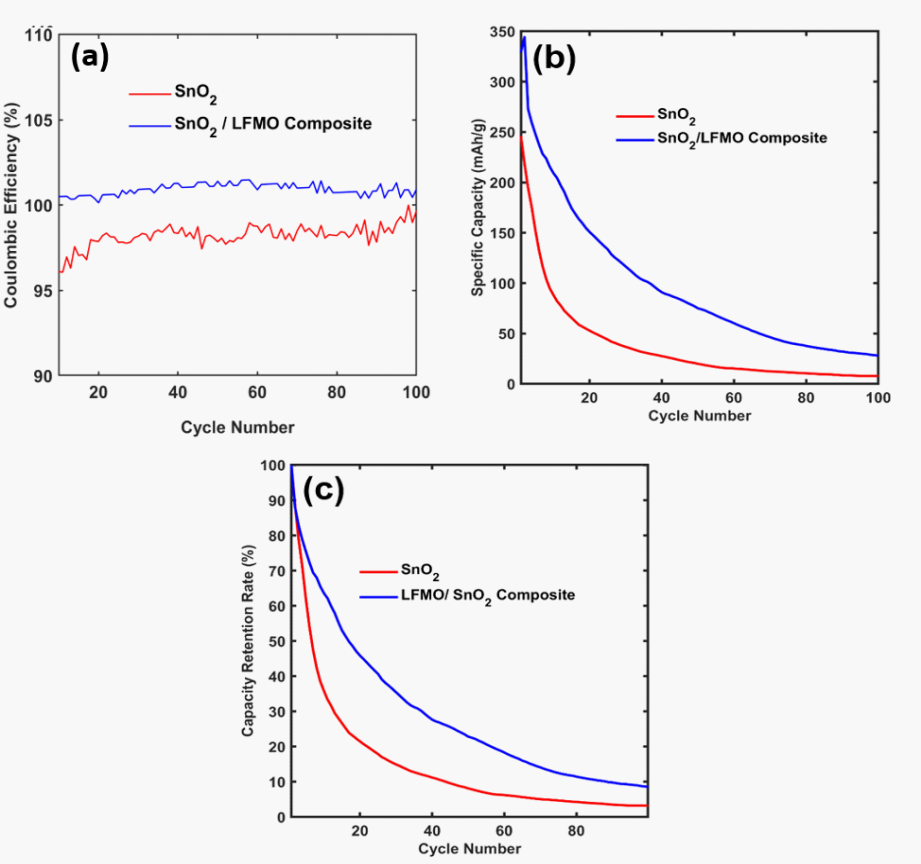

Figure 6. (a) Coulombic efficiencies of LFMO, SnO_2 and SnO_2/LFMO composite (b) Specific capacity vs. cycle number of LFMO, SnO_2 and SnO_2/LFMO composite (c) Capacity retention rate (%) vs. cycle number of LFMO, SnO_2 and SnO_2/LFMO composite.

crystal systems. Figure 4 (b) shows the XRD patterns of the LFMO powder. The peaks revealed the LFMO powder as being in a phase pure spinel structure. The diffraction peaks matched the cubic phase of $Li_2FeMn_3O_8$, which agrees with Kawai et al. (Kawai et al., 1998). Whiles figure 4(c) depicts the XRD pattern of the SnO_2/LFMO composite. Most of the XRD diffraction peaks of the composite material are well matched with the LFMO, as a result of a very thick slurry of LFMO covering the entire surface of the SnO_2 nanorods beneath it. However, a distinct peak of the SnO_2 nanorods orientated along the (101) direction is visible in the composite XRD pattern.

Figure 5 (a) shows the galvanostatic charge and discharge curves of multiple cycles Li-ion coin cell battery made up of SnO_2 electrode at the voltage window between 0.5 V and 3 V. The cell showed a specific capacity of 250 mAh/g during the first charge and discharge cycles. However, it did not maintain significant stability with time at that performance. The charging and discharging capacity decreases as the number of cycles increases, as shown in figure 5 (a). This capacity decrease could be the result of the pulverization of SnO_2 due to severe volume expansion impeding the lithium-ion during the intercalation and de-intercalation process. Furthermore, galvanostatic charge and discharge curves of multiple cycles of the SnO_2/LFMO composite at the voltage window between 0.5 V and 3 V as shown in Figure 5 (b). The coin cell showed a specific capacity of 325 mAh/g initially and gradually lowered its value as the number of cycles increased. However, the specific capacity (mAh/g) of the composite electrode improved significantly compared to the pristine SnO_2, as shown in Figure 5(b).

Figure 6 (a) shows the Coulombic efficiency of SnO_2 and SnO_2/LFMO composite. The pristine SnO_2 is approximately 95% whiles the SnO_2/LFMO composite Coulombic efficiency is steady at 100%. Figure 6 (b) shows the specific capacity vs. cycle number of SnO_2 and SnO_2/LFMO composite electrode. The initial discharge capacity of the pristine SnO_2 is 250 mAh/g and the capacity decreases significantly during the first 100 cycles. On the other hand, the

SnO_2/LFMO composite electrode material exhibits interesting capacitance behavior with a specific discharging capacity of 325 mAh/g. In addition, the battery shows the capacitance value of 325 mAh/g during the 100th cycle of operation, which is an indication that the SnO_2/LFMO composite improved the discharging rate of the pristine SnO_2. This improvement could be attributed to the carbonaceous material, which is added to the LFMO, acting as an ideal volume change buffer as well as a good electron conductor (Wang et al., 2015). According to Hudaya et al., carbonaceous material plays an essential role in the prevention of aggregation of SnO_2 nanoparticles during the lithiation and delithiation process (Hudaya et al., 2015). Figure 6 (c) shows the relations of cycle number with a capacity retention of SnO_2 and SnO_2/LFMO composite electrode.

Conclusion

The preparation and the electrochemical characterization of pristine SnO_2 nanorods and SnO_2/LFMO composite electrodes are investigated systematically. The as-prepared electrode is used to fabricate a coin cell Li-ion battery. The electrochemical characterization of the constructed coin cell is used to determine the specific capacity of the electrodes and their behavior as a function of current density. The results show that the addition of the LFMO to SnO_2, to form the composite electrode, increases the discharging capacity of the SnO_2/LFMO to 325mAh/g, an increase of ~ 30% than that of the SnO_2 electrodes. In addition, we can improve the retention rate of the SnO_2 nanorods by forming a composite with the LFMO.

Acknowledgements

This work is supported by NSF-CREST Grant No. 1036494 and NSF-CREST Grant No: 1547771.

References

Arico AS, P Bruce, B Scrosati, JM Tarascan, and W Van Schalkwijk (2005) Nanostructured materials for advance energy conversion and storage devices. Nat. Mater. 4: 366-377.

Asiedu A, E Barbera, R Naurzaliyev, A Bertucco, and S Kumar (2019) Waste cooking oil to jet-diesel fuel range using 2-propanol via catalytic transfer hydrogenation reactions. Biofuels. https://doi.org/10.1080/17597269.2018.1532754.

Carvajal CG, SRout, R Mundle, and AK Pradhan (2017) Multilayered Approach for TiO_2 Hollow-Shell-Protected SnO_2 Nanorod Arrays for superior lithium storage. Langmuir 33 (1): 11-18.

Dai G, H Du, S Wang, J Cao, M Yu, Y Chen, Y Tang, A Lia, and Y Chena (2016) Improved electrochemical performance of LiNi0.8Co0.15Al0.05O2 with ultrathin and thickness controlled TiO2 shell via atomic layer deposition technology. RSC Adv. 6: 100841–100848. doi: 10.1039/C6RA21903A.

D3242-11, A, (2017) Standard Test Method for Acidity in Aviation Turbine Fuel. ASTM International: West Conshohocken, PA, USA.

Ebin B, M Petranikova, BM Steenari, and C Ekberg (2017) Investigation of zinc recovery by hydrogen reduction assisted pyrolysis of alkaline and zinc-carbon battery iste. Iste Management 68: 508-517.

Guan C, X Wang, Q Zhang, Z Fan, H Zhang, and HJ Fan (2014) Highly stable and Reversible Lithium ion storage in SnO_2 nanowires Surface coated with a Uniform Hollow Shell by Atomic Layer Deposition. Nano letter 14: 4852-4858.

Han X, Y Gong, K Fu, X He, GT Hitz, J Dai, A Perase, B Liu, H Wang, G Rubloff, Y Mo, V Thangadurai, ED Ischsman, and L Hu (2017) Negating interfacial impedance in garnet-based solid-state Li metal batteries. Nature Materials 16: 572–579.

He X, C Du, B Shen, C Chen, X Xu, and Y Wang (2017) Electronically conductive Sb-doped SnO_2 nanoparticles coated LiNi0.8Co0.15Al0.05O2 cathode material with enhanced electrochemical properties for Li-ion batteries. Electrochim. Acta 236: 273–279. doi: 10.1016/j.electacta.2017.03.215.

Hudaya C, JH Park, JK Lee, and W Choi (2014) SnO_2-coated $LiCoO_2$ cathode material for high-voltage applications in lithium-ion batteries. doi:10.1016/j.ssi.2014.01.016.

Jiang HY, L Li, C Yan, C Lee, P See, and J Ma (2011) High–rate electrochemical capacitors from highly graphitic carbon–tipped manganese oxide/mesoporous carbon/manganese oxide hybrid nanowires. Energy Environ. Sci. 4: 1813. doi: 10.1039/c1ee01032h.

Kawai H, M Nagata, MH Tukamoto, and A West (1998) Novel 5V Spinel cathode $Li_2FeMn_3O_8$ for lithium ion batteries. Chem. Mater.10, 32663268.

Lacy F (2011) Developing a theoretical relationship between electrical resistivity, temperature, and film thickness for conductors. Nanoscale Research Letters 6 (1): 636.

Lai YQ, M Xu, Z Zhang, C Gao, P Wang, and Z Yu (2016) Optimized structure stability and electrochemical performance of LiNi0.8Co0.15Al0.05O2 by sputtering nanoscale ZnO film. J. Power Sources 309: 20–26. doi: 10.1016/j.jpowsour.2016.01.079.

Lee SH, CS Yoon, K Amine, and YK Sun (2013) Improvement of long-term cycling performance of Li[Ni0.8Co0.15Al0.05] O2 by AlF3 coating. J. Power Sources 234, 201–207. doi: 10.1016/j.jpowsour.2013.01.045.

Liu J and L Xue-Wei (2012) Two- dimensional nanoarchitectures for lithium storage. Adv. Mater 24: 4097-4111.

Liua W, X Lia, D Xiong, Y Hao, J Li, H Kou, B Yan, D Li, S Lu, A Koo, K Adair, and X Sun (2018) Significantly improving cycling performance of cathodes in lithium ion batteries: the effect of Al_2O_3 and $LiAlO_2$ coatings on LiNi0.6Co0.2Mn0.2O2. Nano Energy 44: 111–120. doi: 10.1016/j.nanoen.2017.11.010.

Lowell, J.E.S. Seymour, M. A. T., Matthias Thommes. (2006). Characterization of Porous Solids and Powders: Surface Area, Pore Size and Density. 4th edition ed.; Springer: The Netherlands.

Pan H, S Zhang, J Chen, M Gao, Y Liu, T Zhu, and Y Jiang (2018) Li- and Mn-rich layered oxide cathode materials for lithium-ion batteries: a review from fundamentals to research progress and applications. Mol. Syst. Des. Eng. 3 (5): 748-803.

Patel P and L Gaines (2016) Recycling Li batteries could soon make economic sense. MRS Bulletin 41 (6): 430-431.

Tirupath RP, D Shanmughasundaram, B Kishore, AV Jeyaseelan, AK Subramani, and N Munichandraiah (2016) Composite of Li-Rich Mn, Ni and Fe Oxides as Positive Electrode Materials for Li-Ion Battery. J. Electrochem. Soc.163 A1493.

Poizot P, S Laruelle, S Grugeon, L Dupont, and JM Tarascon (2000) Nano-sized transition-metaloxide as negative-electrode materials for lithium-ion batteries. Nature 407: 496-499.

Sharma AP, P Dhakal, DK Pradhan, MK Behera, B Xiao, and M Bahoura (2018) Fabrication and characterization of SnO_2 nanaorods for room temperature gas sensor. AIP Advances 8: 095219. doi:10.1063/1.5050991.

Si C, J Zhou, and Z Sun (2015) Half-Metallic Ferromagnetism and Surface Functionalization-Induced Metal–Insulator Transition in Graphene-like Two-Dimensional Cr2C Crystals. doi: 10.1021/acsami.5b05401.

Srur-Lavi O, V Miikkulainen, B Markovsky, J Grinblat, M Talianker, and Y Fleger (2017) Studies of the electrochemical behavior of $LiNi_{0.8}Co_{0.15}Al_{0.05}O_2$ electrodes coated with $LiAlO_2$. J. Electrochem. Soc. 164, A3266–A3275. doi: 10.1149/2.1631713jes.

Tabuchi M, A Nakashima, K Ado, H Kageyama, and K Tatsumi (2005) Heat-Treatment Effect on Phase Stability, Cation Distribution, Chemical Composition, and Electrochemical Behavior for Fe-Substituted Li2MnO$_3$. doi:10.1021/cm050095+.

Tarascon JM and M Armand (2001) Issues and challenges facing rechargeable lithium batteries. Nature 414: 359-367.

Wang C, W Peng, Z Li, Y Liang, S Zhong, and Q Zhang (2019) Synthesis and Characterization of Nano SnO_2 Modification on $LiNi_{0.8}Mn_{0.1}Ni_{0.1}O_2$ Cathode Materials for Lithium Ion Batteries. Energy Res. 7:125. doi: 10.3389/fenrg.2019.00125.

Wang HG, DL Ma, XL Huang, Y Huang, and XB Zhang (2012) General and controllable synthesis of metal oxide/TiO2 hierarchical heterostructures with improved lithium-ion battery performance. Sci. Rep. 2: 481.

Wang J, C Du, C Yan, X He, B Song, G Yin, P Zuo, and X Cheng (2015) Al_2O_3 Coated concentration-gradient $Li[Ni_{0.73}Co_{0.12}Mn_{0.15}]O_2$ cathode material by freeze drying for long-life lithium ion batteries. Electrochim. Acta 174: 1185–1191. doi: 10.1016/j.electacta.2015.06.112.

Wang X, B Liu, Q Wang, W Song, X Hou, D Chen, and G Shen (2013). Three-dimensional hierarchical $GeSe_2$ nanostructures for high performance flexible all-solid-state super capacitors. Adv. Mater. 25: 1479-1486.

Wang X, Q Xiang, B Liu, L Wang, T Luo, D Chen, and G Shen (2013) TiO_2 modified FeS Nanostructured with Enhanced Electrochemical Performance for Lithium-Ion Batteries. Scientific Reports 3, 2007.

Wang Y, Z Huang, Y Shi, JI Wong, M Ding, and Y Ying (2015) Designed hybrid nanostructure with catalytic effect: beyond the theoretical capacity of SnO_2 anode material for lithium ion batteries. Scientific Reports 5, 9164. doi: 10.1038/srep09164.

Wu F, X Zhang, T Zhao, L Li, M Xie, and R Chen (2015) Surface modification of a cobalt-free layered Li $[Li_{0.2}Fe_{0.1}Ni_{0.15}Mn_{0.55}]O_2$ oxide with the $FePO_4/Li_3PO_4$ composite as the cathode for lithium-ion batteries. J. Mater. Chem. A 3 (18): 9528-9537.

Xie ZC, YY Zhang, AB Yuan, and JQ Xu (2019) Effects of lithium excess and SnO_2 surface coating on the electrochemical performance of $LiNi_{0.8}Co_{0.15}Al_{0.05}O_2$ cathode material for Li-ion batteries. J. Alloy Comp. 787: 429–439. doi: 10.1016/j.jallcom.2019.02.127.

Xu C, Y Zeng, X Rui, N Xiao, J Zhu, W Zhang, J Chen, W Liu, H Tan, HH Hng, and Q Yan (2012) Controlled soft-template synthesis of ultrathin C @ FeS nanosheets with high –Li-storage performance. ACS Nano 6 (6): 4713-4721.

Zhao Y, Y Wang, C Ji, Z Zhaoa, and Z Lva (2016) Electrochemistry and structure of Li-rich cathode composite: $Li_{1.26}Fe_{0.22}Mn_{0.52}O_2$ in situ integrated with conductive network graphene oxide for lithium-ion batteries. RSC Adv. 6 (38): 31762-31768.

Zheng J, Z Yang, Z He, H Tong, W Yu, and J Zhang (2018) In situ formed LiNi0.8Co0.15Al0.05O2@Li4SiO4 composite cathode material with high rate capability and long cycling stability for lithium-ion batteries. Nano Energy 53: 613–621. doi: 10.1016/j.nanoen.2018.09.014.